

## Transition from Boundary- to Bulk-Controlled Regimes in Optical Pattern Formation

F. T. Arecchi,<sup>(a)</sup> S. Boccaletti, P. L. Ramazza, and S. Residori

*Istituto Nazionale di Ottica, 50125 Firenze, Italy*

(Received 9 November 1992)

By increasing the Fresnel number  $F$  of the cavity of a photorefractive oscillator, we report the transition from a boundary-controlled regime, where the size of the transverse patterns scales as  $1/\sqrt{F}$ , to a bulk-controlled regime where the pattern size is independent of  $F$ . In this new regime, the size corresponds to an intrinsic correlation length imposed by diffusion processes within the material. The wave number spectrum of the emitted field has a sharp cutoff, corresponding to the length scale of bulk correlations. Such a new behavior is explained by the wave number dependence of the gain within the instability region.

PACS numbers: 42.50.Lc, 05.45.+b

Two types of pattern formation can arise in a system far from equilibrium, namely, the forced one, where the symmetry is imposed through the boundary, either by the geometry or by an external driving force, and the spontaneous one, where the symmetry is imposed by the bulk parameters of the active medium without any boundary influence.

Examples of the first type are convective instabilities in fluids, where the scale length is imposed by the cell height [1] or the capillary pattern in fluid layers submitted to a periodic vertical force (Faraday instability) [2,3].

A Turing instability is the prototype of a bulk instability [4]. Indeed let us consider a reaction-diffusion process with two competing species  $i=1,2$  with diffusion lengths  $l_i$ , reacting through a nonlinear coupling. If we adjust the coupling in order to have an activator ( $i=1$ ) and an inhibitor ( $i=2$ ), then in the limit  $l_1/l_2 \ll 1$  stationary patterns may arise with a scale length of the order of  $\Lambda \sim (l_1 l_2)^{1/2}$ , independent of the boundary [5]. Only recently [6] has experimental evidence of chemical Turing patterns been offered, since beforehand transport effects were stirring the chemical components, thus imposing a boundary dependence.

In this Letter we report optical pattern formation for different "aspect ratios" (i.e., different Fresnel numbers), showing the transition from patterns dominated by the geometric parameters to patterns whose scale length is imposed by the bulk properties of the medium.

In the case of optical media, any device based on the original Schawlow-Townes idea [7] of mode selection in a cavity much larger than the optical wavelength  $\lambda$  yields transverse patterns depending upon the so-called Fresnel number  $F = a^2/\lambda L$ .  $F$  includes the two relevant geometrical parameters, namely, the transverse size  $a$  and the longitudinal size  $L$  of the cavity, and it accounts for competition between geometric acceptance and diffraction phenomena. As a result, patterns based upon optical propagation are boundary dominated, even though sometimes called "Turing phenomena" [8]. Indeed, observed patterns in lasers can be explained exclusively in terms of symmetries imposed by the boundary [9].

Recent evidence of transverse optical patterns in a pas-

sive alkali cell showed hexagon formation, but the experiment was carried out at fixed geometrical parameters [10] and no hints were offered on possible boundary-bulk tradeoff. Another experiment on an optical cavity with a dephasing slab of liquid crystals [11] showed patterns scaling with the cavity length in a purely diffractive way.

Our experiment is carried out on a photorefractive oscillator consisting of a ring cavity of length  $L$  containing a thin photorefractive BSO crystal pumped by an argon laser [12]. The two-wave mixing between pump and cavity fields provides a grating of refractive index which couples the two fields by Bragg scattering. For increasing Fresnel numbers, we have the successive onset of two regimes, a first one which displays space coherence, where single cavity modes alternate sequentially, either periodically or chaotically, and a second one of spatiotemporal chaos, where a mode mixing appears with a consequent reduction of the coherence length.

A fundamental geometric parameter of this experiment is the spot size of the central mode which is constrained by the quasiconfocal configuration (intracavity lens of focal length  $L/4$ , positioned at a distance from the crystal close to  $L/4$ ). Thus, the spot size of the central mode is given by [13]

$$w_0 = \sqrt{\lambda L / \pi}. \quad (1)$$

Provided the mirror size  $a$  is larger than  $w_0$ , that is, that the Fresnel number  $F = a^2/\lambda L$  is larger than 1, the cavity can house higher order modes, made of regular arrangements of bright spots (peaks of Gauss-Laguerre functions in cylindrical geometry) of size

$$D \approx w_0 / \sqrt{F}. \quad (2)$$

Since the overall spot size of a transverse mode of order  $n$  scales as  $\sqrt{n} w_0$ , it is clear that  $n = F$  is the largest order mode compatible with the boundary conditions (filling of all the aperture area).

In order to check experimentally such a scaling law, we rely on the fact that patterns built by superposition of Gauss-Laguerre functions have in general an average size  $D$  of bright peaks equal to the average separation  $\langle D \rangle$  of zero intensity points [13]. Furthermore, each intensity

zero provides a phase singularity [14], which can be detected as a fringe dislocation by heterodyning with a tilted reference plane wave. In this way [15] we provide a technique for measuring the average nearest neighbor separation  $\langle D \rangle$  between phase singularities, which represents the characteristic length of our pattern system.

A plot of  $\langle D \rangle$  vs  $F$  [Fig. 1(a)] shows that Eq. (2) is verified up to a critical value  $F_c$ , above which  $D$  is almost independent of  $F$ . In a similar way, the total number  $N$  of phase singularities scales as  $F^2$  or  $F$ , respectively, below and above  $F_c$ . This transition is evident in Fig. 1(b) and its root is the following.  $N$  is the ratio of the total wave-front area  $a^2$ , which scales as  $F$ , to the area  $\langle D \rangle^2$  containing a single phase singularity, which scales as  $F^{-1}$  or  $F^0$ , respectively, below and above  $F_c$ .

We can understand the transition as follows. Consider the photorefractive crystal as a collection of uncorrelated optical domains, each one with a transverse size limited by a correlation length  $l_c$  intrinsic of the crystal excitations [16]. Then the medium gain has an upper cutoff at a transverse wave number  $1/l_c$  and spatial details are

amplified only up to that frequency, that is, provided they are bigger than  $l_c$ . Thus, for a critical  $F_c$  such that  $D = w_0/F_c^{1/2} = l_c$  we expect a transition from a boundary-dominated regime described by Eq. (2) to a bulk-dominated regime whereby the separation of the phase singularities is independent of  $F$ . This is indeed the case as shown in Fig. 1, which yields a value  $F_c \approx 11$  corresponding to  $l_c \approx 170 \mu\text{m}$ , since  $w_0 \approx 600 \mu\text{m}$  for  $L = 200 \text{ cm}$ .

The reduction of the boundary influence is also signaled by the reduction of the topological charge imbalance. Indeed, since a regular field should have a balance between topological charges of different sign [14], an imbalance means that two phase singularities of opposite sign have been created close to the boundary and only one has remained within the boundary. Therefore, there is a boundary layer of area  $a\langle D \rangle$  containing  $N_1 \sim a/\langle D \rangle$  singularities ( $N_1 \ll N$  as soon as  $\langle D \rangle \ll a$ ) within which a topological charge imbalance can occur. The absolute value of the imbalance of positive to negative charges is, for statistical reasons, of the order of  $N_1^{1/2}$ , and thus the normalized imbalance is  $U = N_1^{1/2}/N$ . Accounting for the scaling of  $\langle D \rangle$  with  $F$ , it follows that  $U$  scales as  $F^{-1.5}$  and  $F^{-0.75}$ , respectively, below and above  $F_c$ . Figure 2 reports the experimental results which are in agreement with this expectation.

In order to characterize directly  $l_c$ , we measure the single pass gain of BSO in a two-wave mixing configuration without cavity as shown in Fig. 3(a). A lens provides an image of the near-field output on the videocamera VD. A diaphragm on the focal plane of the lens filters out noise. By tilting the two waves, we measure the photorefractive gain  $G_0$  versus the grating spatial frequency  $K$ . As shown in Fig. 3(b) we have the maximum gain for an optimal

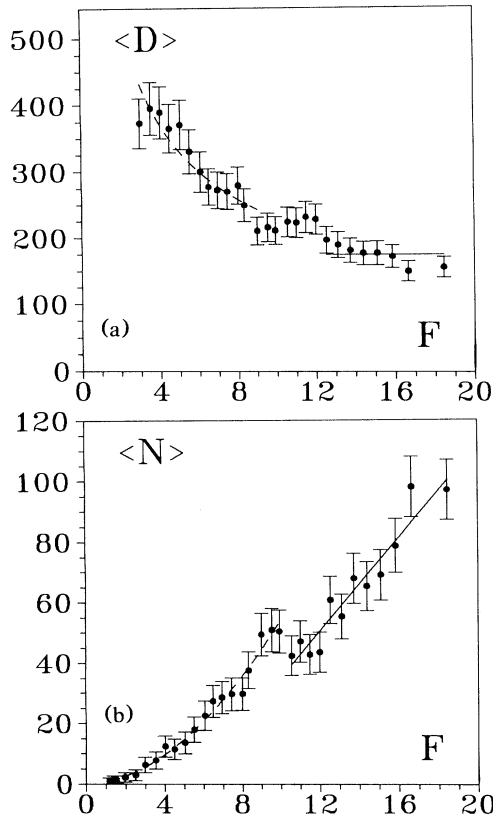


FIG. 1. (a) Mean nearest neighbor separation  $\langle D \rangle$  (scale in  $\mu\text{m}$ ) between phase singularities and (b) average total number  $\langle N \rangle$  of phase singularities vs the Fresnel number  $F$  of the cavity. Dashed lines are best fits with the boundary-dependent scaling laws  $\langle D \rangle \sim F^{-1/2}$  and  $\langle N \rangle \sim F^2$ . Solid lines are best fits with the bulk-dominated scaling laws  $\langle D \rangle \sim F^0$  and  $\langle N \rangle \sim F^1$ .

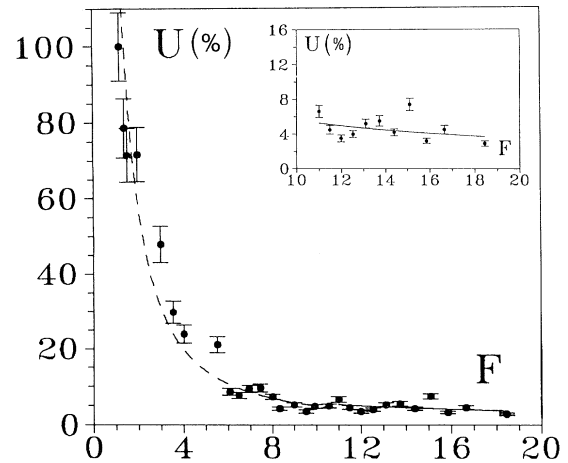


FIG. 2. Average charge imbalance  $U \equiv (|n_+ - n_-| / (n_+ + n_-))$  vs  $F$ .  $n_+$  ( $n_-$ ) is the total number of positive (negative) phase singularities as defined in Ref. [15]. Dashed line:  $F^{-1.5}$  fit up to  $F = 11$ ; solid line:  $F^{-0.75}$  fit from  $F = 11$  on. Inset: Expanded view of the  $F > 11$  region.

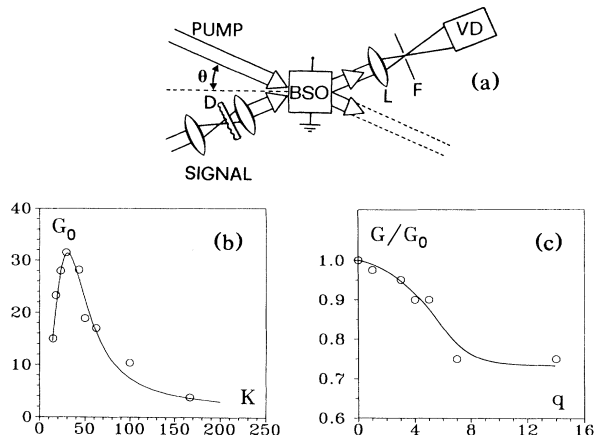


FIG. 3. (a) Experimental setup for measuring the spatial frequency response of BSO.  $D$ : diffuser;  $L$ : lens;  $F$ : diaphragm. (b) Gain  $G_0$  (ratio of the output signal intensities with and without pump) vs  $K$  (measured in  $\text{mm}^{-1}$ ). (c) Gain  $G$  vs spectral broadening  $q$  ( $\text{mm}^{-1}$ ), measured with  $\theta$  fixed at the optimum value. The solid line is an interpolation of the experimental points.

angle  $\theta \sim 1^\circ$  corresponding to a Bragg grating with periodicity  $K^{-1} \sim \lambda/\theta \sim 30 \mu\text{m}$ . The solid line is a best fit according to the photorefractive theory of light scattering [17]. In order to measure  $l_c$ , we have to explore the broadening of the gain peak around  $K$ . When a diffuser is inserted on the signal path, it provides a spectral broadening  $q$ , controlled by translating the diffuser between two confocal lenses. In this way, we measure the amount of amplification of a speckle field of varying size. The data [Fig. 3(c)] yield a cutoff at  $q_c \sim 5 \text{mm}^{-1}$  whose reciprocal is in agreement with the indirect evaluation of  $l_c$ .

A model of pattern formation in a Kerr medium exposed to a pair of counterpropagating fields [18] provides two scale lengths, one  $(\lambda L)^{1/2}$  depending only on diffraction and one  $(\lambda L l_c)^{1/3}$  accounting also for material diffusion over a correlation length  $l_c$ . This latter one, however, still contains the geometric parameter  $L$ , and for sufficiently small  $L$  it would provide a pattern length even smaller than  $l_c$ . In fact, an intrinsic cutoff length does not emerge from that treatment, because saturation effects of the nonlinearity are completely neglected.

In Ref. [12] the range of  $F$  numbers explored was not wide enough to give evidence of two separated regimes; thus we fitted the available data for  $\langle D \rangle$  and  $N$  vs  $F$  with global exponents slightly different from  $-0.5$  and  $2$  ( $-0.62$  and  $1.79$ , respectively). The present extension to larger  $F$  numbers allows clear separation of the two regimes.

Finally, above  $F_c$ , the persistence time  $\langle T \rangle$  of a phase singularity within a domain of size  $\langle D \rangle$  has also to be independent of  $F$ . This was evident in Fig. 6(a) of Ref. [15], although no adequate explanation could be offered at that time.

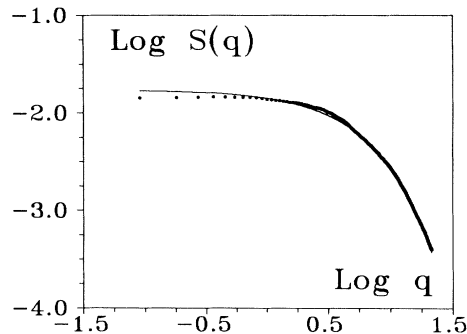


FIG. 4. Field power spectrum  $S(q)$ , measured integrating the signal intensity over concentric shells of radius  $q$  ( $\text{mm}^{-1}$ ) in the Fourier space. Dots: experimental points,  $F=70$ . Solid line: best fit with  $\exp[-(q/q_0)^\beta]$  yielding  $\beta=0.96$ ,  $q_0=5.3 \text{mm}^{-1}$ .

A further independent check of bulk-dominated patterns is given by the power spectrum  $S(q)$  of the transverse optical field for  $F > F_c$ . This measurement is done by integrating the signal intensity over concentric shells of radius  $q$  in the Fourier space provided by the far-field propagation of the cavity field. The results are reported in Fig. 4. The best fit of the data yields an exponential high frequency cutoff  $e^{-q/q_0}$  with  $q_0=5.3 \text{mm}^{-1}$ . This corresponds to a correlation length  $1/q_0 \sim 190 \mu\text{m}$  for the field, in good agreement with the values of  $l_c$  reported above. A broadband spectrum with an exponential cutoff is a clear signature of spatiotemporal chaos [19], where a chaotic dynamics of spatial patterns is involved, with a dominant length scale.

The transition here reported to a boundary-independent regime can be explained as follows. Linearizing the dynamics at the onset of the instability, the gain per unit length  $g(q)$  provided by the crystal for each  $q$  component should be equal to the attenuation  $\alpha(q)$ , in order to have marginal stability.

The attenuation  $\alpha(q)$  is derived by the following considerations. A spectrophotometric measurement gives a transmission  $T_1=37\%$  through the crystal in the absence of pump, corresponding to a linear attenuation  $\alpha_1$ . Furthermore, the optical intracavity elements (beam splitter, lenses) add an attenuation  $1-T_2=20\%$ . Reducing this last one to an equivalent crystal attenuation  $\alpha_2$ , we have  $\exp[-(\alpha_1+\alpha_2)l]=T_1T_2=0.296$ , yielding  $\alpha=\alpha_1+\alpha_2=1.2 \text{cm}^{-1}$ , since the crystal length is  $l=1 \text{cm}$ . Besides this uniform attenuation there is a  $q$ -dependent attenuation  $\alpha_d(q)$  due to the diffractive spread of the beam, so that the overall attenuation is  $\alpha(q)=\alpha+\alpha_d(q)$ . A beam of radius  $r$  at the crystal exit reenters after a cavity round trip of length  $L$ , with a radius increased by diffraction. The  $q$  component of the field [diffraction angle  $\theta(q)=q/k$ , where  $q$  and  $k=1/\lambda$  are the lengths of the transverse and longitudinal wave vectors] will be spread over a radius  $r+Lq/k$ , thus the relative loss due to the limited crystal aperture is

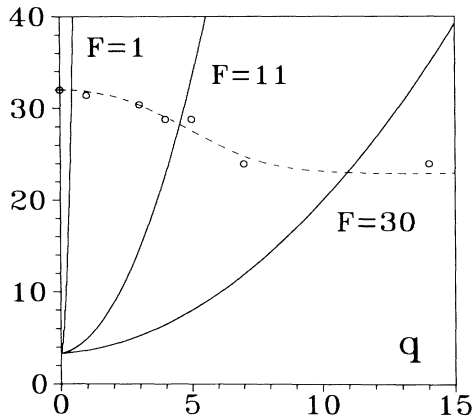


FIG. 5. Marginal stability curves vs  $q$  for different Fresnel numbers (solid lines) and gain curve (dashed line). For convenience we have reported the global gain  $G(q)$  and the inverse transmissions  $T^{-1}(q)$ , rather than  $g(q)$  and  $\alpha(q)$ .

$$1 - e^{-\alpha_d(q)l} = \frac{(r + Lq/k)^2 - r^2}{(r + Lq/k)^2}. \quad (3)$$

From this relation,  $\alpha_d(q)$  can be derived for different Fresnel numbers  $F = r^2/\lambda L$ . In Fig. 5 we report the marginal stability curves  $\alpha(q) = \alpha + \alpha_d(q)$  vs  $q$  for different  $F$  and compare them with the actual gain per unit length  $g(q)$  obtained from the data of Fig. 3(c) as follows. Figure 3(b) gives the ratio of the transmission in axis with and without pump, which amounts to  $G_0 = \exp(g_0 l)$ , thus yielding  $g_0 = 3.5 \text{ cm}^{-1}$  at the peak  $G_0 = 32$ . An observer placed at a propagation angle  $q/k$  detects a reduced gain  $G(q) = \exp[g(q)l]$  as plotted in Fig. 3(c), from which we deduce  $g(q)$ .

As can be seen in Fig. 5, for low Fresnel numbers the gain curve is practically flat, therefore the mode selection depends exclusively on  $\alpha(q)$ , that is, on the boundary symmetries; thus it is irrelevant to worry for a detailed material model [20]. On the contrary, for  $F > 10$  the gain cutoff at  $q_c = 1/l_c \sim 5 \text{ mm}^{-1}$  constrains the minimum spot size, independently from the maximal  $q$  allowed by the marginal stability curve. In fact, while the linear stability analysis enables all modes within the marginal curve to oscillate, the nonlinear coupling selects those close to the gain peak, that is, confined within the half-width of the gain curve.

Even though here presented for an optical system, the boundary-bulk tradeoff is very general and it holds for any pattern forming system. Only in the presence of a broadband gain mechanism we can assume that the mode selection is controlled by the marginal stability curve. A gain cutoff reduces the boundary influence and introduces the medium dynamics as the relevant agent of pattern formation.

We are grateful to P. Coulet and N. R. Heckenberg for useful discussions. This work had a partial support from EEC-Esprit Basic Research action TONICS (Con-

tract No. 7118).

<sup>(a)</sup>Also Department of Physics, University of Firenze, Firenze, Italy.

- [1] P. Manneville, *Dissipative Structures and Weak Turbulence* (Academic, San Diego, CA, 1990).
- [2] A. B. Ezerskii, P. I. Korotin, and M. I. Rabinovich, *Pis'ma Zh. Eksp. Teor. Fiz.* **41**, 129 (1985) [*JETP Lett.* **41**, 157 (1985)]; N. Tuffiaro, R. Ramshankar, and J. P. Gollub, *Phys. Rev. Lett.* **62**, 422 (1989).
- [3] Recently, however, experimental evidence was given of a transition from a boundary dominated to a bulk-dominated Faraday pattern for a liquid-vapor interface close to the critical point: S. Fauve, K. Kumar, C. Laroche, D. Beysens, and Y. Garrabos, *Phys. Rev. Lett.* **68**, 3160 (1992).
- [4] A. M. Turing, *Philos. Trans. R. Soc. London* **237**, 37 (1952).
- [5] B. S. Kerner and V. V. Osipov, *Usp. Fiz. Nauk* **162**, 1 (1990) [*Sov. Phys. Usp.* **33**, 679 (1990)].
- [6] V. Castets, E. Dulos, J. Boissonade, and P. De Kepper, *Phys. Rev. Lett.* **64**, 2953 (1990).
- [7] A. L. Schawlow and C. H. Townes, *Phys. Rev.* **112**, 1940 (1958).
- [8] L. A. Lugiato and L. Lefever, *Phys. Rev. Lett.* **58**, 2209 (1987).
- [9] C. Green, G. B. Mindlin, E. J. D'Angelo, H. G. Solari, and J. R. Tredicce, *Phys. Rev. Lett.* **65**, 3124 (1990).
- [10] G. Grynberg, E. Le Bihan, P. Verkerk, P. Simoneau, J. R. R. Leite, D. Bloch, S. Le Boiteux, and M. Ducloy, *Opt. Commun.* **67**, 363 (1988); A. Petrossian, M. Pinard, A. Maitre, J.-Y. Courtois, and G. Grynberg, *Europhys. Lett.* **18**, 689 (1992).
- [11] R. Macdonald and H. J. Eichler, *Opt. Commun.* **89**, 289 (1992).
- [12] F. T. Arecchi, G. Giacomelli, P. L. Ramazza, and S. Residori, *Phys. Rev. Lett.* **65**, 2531 (1990).
- [13] H. Kogelnik, in *Lasers: A Series of Advances*, edited by A. K. Levine (Dekker, New York, 1966).
- [14] M. Berry, in *Physics of Defects*, edited by R. Balian *et al.* (North-Holland, Amsterdam, 1981), pp. 456-543.
- [15] F. T. Arecchi, G. Giacomelli, P. L. Ramazza, and S. Residori, *Phys. Rev. Lett.* **67**, 3749 (1991).
- [16] Even though not essential for the purposes of this paper, we recall that the decorrelation mechanism in a photorefractive crystal is due to the diffusion of the space charge wave which provides the refractive index grating. The decorrelation length measured here coincides with the diffusion length, as discussed in detail in F. T. Arecchi, S. Boccaletti, G. Giacomelli, G. P. Puccioni, P. L. Ramazza, and S. Residori, *Physica (Amsterdam) D* (to be published).
- [17] P. Günter and J. P. Huignard, *Photorefractive Materials and their Applications* (Springer-Verlag, Berlin, 1988).
- [18] G. D'Alessandro and W. J. Firth, *Phys. Rev. A* **46**, 537 (1992).
- [19] Y. Pomeau, A. Pumir, and P. Pelce, *J. Stat. Phys.* **37**, 39 (1984); P. C. Hohenberg and B. J. Shraiman, *Physica (Amsterdam)* **37D**, 109 (1989).
- [20] F. T. Arecchi, S. Boccaletti, G. B. Mindlin, and C. Perez Garcia, *Phys. Rev. Lett.* **69**, 3723 (1992).